Journal of Hydrology 590 (2020) 125543

Contents lists available at ScienceDirect

Journal of Hydrology

journal homepage: www.elsevier.com/locate/jhydrol

Research papers

# Geochemical responses of cave drip water to vegetation restoration

Yina Lyu[a,b], Weijun Luo[c,a,d,*], Yanwei Wang[a,b], Guangneng Zeng[e], Xianli Cai[a,b,d], Meifang Wang[a,b], Jia Chen[a,b,d], Kaiping Yang[a,b], Xu Weng[a,b], Anyun Cheng[a,d], Lin Zhang[a,d], Runyu Zhang[a], Shijie Wang[a,d]

[a] State Key Laboratory of Environmental Geochemistry, Institute of Geochemistry, Chinese Academy of Sciences, Guiyang 550081, China
[b] University of Chinese Academy of Sciences, Beijing 100049, China
[c] Guizhou Provincial Key Laboratory of Geographic State Monitoring of Watershed, Guizhou Education University, Guiyang 550018, China
[d] Puding Karst Ecosystem Research Station, Chinese Academy of Sciences, Puding 562100, China
[e] School of Eco-Environmental Engineering, Guizhou Minzu University, Guiyang 550025, China

ARTICLE INFO

This manuscript was handled by C. Corradini, Editor-in-Chief

*Keywords:*
Stable isotopes
Elements/ions
Drip water
Vegetation restoration

ABSTRACT

The transmission of stable isotopes and elements/ions from the outside to the inside of a cave and their incorporation into drip water can involve numerous biogeochemical processes. To understand how the original signals of stable isotopes and elements/ions are modified by these processes, integrated studies of the interactions between vegetation, soil, epikarst, and caves are required. We conducted a multi-year monitoring study of the vegetation biomass, tree breast-height diameter, $P_{CO_2}$ in soil air and cave air, $\delta^{13}C$ in soil air, stable oxygen isotope in rainwater and drip water, and stable carbon isotope and elements/ions concentrations in drip water in Shawan Cave system, southwest China. The main results were as follows: (1) The evaporation effect weakened and the transpiration effect strengthened outsides the cave as vegetation improved, thus leading to a year-by-year increasing trend in the $\delta^{18}O$ value of drip water. This indicates that changes in vegetation may have been another potential factor influencing the interannual variation of the $\delta^{18}O$ value of drip water. (2) The $CO_2$ concentration and $\delta^{13}C$ value in soil air increased and decreased, respectively, with vegetation restoration, which caused the interannual variation in the dissolved inorganic carbon isotope ($\delta^{13}C_{DIC}$) value of drip water during the autumn and winter to exhibit a year-by-year decreasing trend. (3) The variations in the elements/ions concentrations of drip water were affected by vegetation uptake, vegetation transpiration, and water–rock interactions. It is inferred that the interannual variation in the elements/ions concentrations of drip water responded to vegetation restoration. (4) A conceptual model demonstrated that the three response modes of drip water $\delta^{18}O$ value, $\delta^{13}C_{DIC}$ value, and elements/ions to variations in vegetation. Overall, this study highlights the responses of the interannual changes in $\delta^{13}C_{DIC}$, $\delta^{18}O$, and elements/ions of drip water to vegetation restoration, which contributes critical insights into the paleoenvironmental interpretation of proxies of speleothems.

## 1. Introduction

The stable isotopes ($\delta^{18}O$ and $\delta^{13}C$) and trace elements of speleothems have been widely used as proxies for the paleoenvironmental signal (Baskaran and Krishnamurthy, 2013; Cosford et al., 2008; Fairchild and Treble, 2009). Speleothem $\delta^{18}O$ may chiefly reflect the changes in moisture sources, transport pathways, intensity of Asian summer monsoon, rainout effect, and convection intensity (Duan et al., 2016; Zhang and Li, 2019; Liu et al., 2020). Whereas carbon isotopes are usually employed to reconstruct changes in vegetation (Cosford et al., 2009). Trace elements can complement stable isotopes data, and can also be used to reconstruct environmental changes (Casteel and Banner, 2015; Fairchild and Treble, 2009; Zhang and Li, 2019). In particular, the $\delta^{18}O$ value of speleothems is closely linked to hydrological processes (Sun et al., 2018; Zhang and Li, 2019). The hydrogeochemical processes of drip water can impact the $\delta^{13}C$ value and trace element composition of speleothems to a certain extent (Fairchild et al., 2006; Frisia et al., 2011; Liu et al., 2017), and numerous studies have indicated that the appeal of speleothems $\delta^{13}C$ and trace elements exists in their sensitivity to biogeochemical processes (Li and Li, 2018; Treble et al., 2016).

The effects of biogeochemical processes on the $\delta^{13}C$ value and trace element composition of speleothems have been confirmed by numerous studies (Benedetti et al., 2003; Drever and Smith, 1978; Dogramaci and

* Corresponding author at: State Key Laboratory of Environmental Geochemistry, Institute of Geochemistry, Chinese Academy of Sciences, Guiyang 550081, China.
*E-mail address:* luoweijun@vip.gyig.ac.cn (W. Luo).

https://doi.org/10.1016/j.jhydrol.2020.125543

Available online 16 September 2020

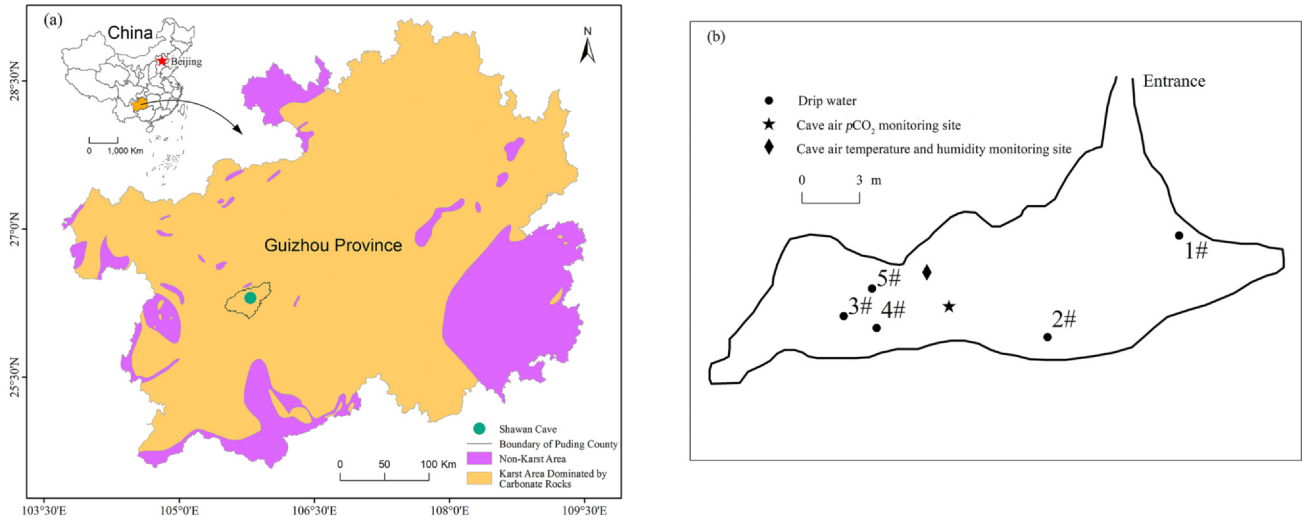


**Fig. 1.** (a) Geographical location of Shawan Cave. (b) Sectional view map of Shawan Cave. Distribution of drip water including 1#, 2#, 3#, 4#, and 5# (solid black circle).

Herczeg, 2002). The change in the $\delta^{13}C$ value of speleothems may reflect changes in regional vegetation. There are two main reasons for this: on the one hand, the $\delta^{13}C$ value of soil air is controlled by the vegetation biomass, and the $\delta^{13}C$ signal in speleothems can be inherited from the $\delta^{13}C$ of soil air (Baker et al., 1997; Cerling, 1984; Mattey et al., 2016); hence, the $\delta^{13}C$ value of speleothems can retain information relating to local vegetation. On the other hand, the different photosynthetic pathways of different vegetation types cause vegetation to have different $\delta^{13}C$ values, which leads to different $\delta^{13}C$ values in speleothems (McDermott, 2004). This can mean that different $\delta^{13}C$ values in speleothems represent different types of vegetation. The trace elements in speleothem are influenced by the trace element composition of the soil zone (Fairchild and Frisia, 2013; Hartland et al., 2012; Rutlidge et al., 2014). Further, changes in trace elements from the soil zone are linked to fluorescent organic matter (Baker et al., 2008) and a historic episode of deforestation (Borsato et al., 2007). This leads to the release and uptake of elements as nutrients by vegetation, and determines the effect of the vegetation dynamics on speleothem chemistry (Borsato et al., 2015; Treble et al., 2016). Thus, these processes that are related to vegetation result in variations in the trace element signals of speleothems. Additionally, the $\delta^{18}O$ values of speleothems at Brown's Folly Mine were found to be neither controlled by the surface temperature nor the seasonal rainfall distribution, which was affected by the vegetation density (Baldini et al., 2005). This suggests that biogeochemical processes could also lead to variations in the $\delta^{18}O$ value of speleothems.

Although many studies that used drip water as a research object have indicated that the stable isotopes and trace elements of speleothems respond to vegetation change, these studies usually used a spatial approach instead of a temporal approach (Luo et al., 2013; Surić et al., 2018; Wassenburg et al., 2020). The limitation of a spatial approach is that the paleoenvironmental implications of these studies are deduced. Hence, it might not be possible to directly demonstrate the responses of the stable isotopes and trace elements of speleothems to variations in vegetation on a temporal scale via this approach. Moreover, most studies only analyzed a single proxy in drip water (Duan et al., 2016; Li and Li, 2018; Treble et al., 2016), and comprehensive studies combining $\delta^{13}C$, $\delta^{18}O$, and element/ion data have been rarely reported.

Since the late 1990s, the Natural Forest Protection Project, the Grain to Green Program, and the Karst Rocky Desertification Comprehensive Control project have been implemented in China (Liu et al., 2014; Qi et al., 2013; Tong et al., 2017). These projects have led to increasing aboveground biomass in the karst regions of southwest China. Furthermore, the biomass may cause increasing trends in the potential carbon mass and trace element concentrations in the soil and subsurface, which might ultimately cause a change in the hydrological conditions of caves (Bourges et al., 2020). These karst regions, therefore, offer an opportunity to directly study the responses of stable isotopes and elements/ions of drip water to vegetation change. In order to understand the impact of biogeochemical processes on drip water hydrogeochemistry, comprehensive research on the migration mechanism of stable isotopes and elements/ions in the cave systems of natural restoration karst regions needs to be carried out based on multi-year cave monitoring.

In this study, multi-year monitoring was undertaken at Shawan Cave, Puding County, Guizhou Province, southwest China. The monitoring included measurements of the vegetation biomass, tree breast-height diameter, $P_{CO_2}$ of soil air and cave air, $\delta^{13}C$ values in soil air and drip water, $\delta^{18}O$ and $\delta^{2}H$ in rainwater and drip water, and elements/ions concentrations in drip water. The fitted sine function relationship between $\delta^{18}O$ values of drip water and $\delta^{18}O$ values of rainfall was used to estimate the mean residence times of drip water. Principal components analysis (PCA) was used to determine the main processes influencing the change in the elements/ions concentrations of drip water. The objectives of this study are to (1) investigate the interannual variations in the dissolved inorganic carbon isotope ($\delta^{13}C_{DIC}$) value and elements/ions concentrations of drip water, and the seasonal and interannual variations in the $\delta^{18}O$ value of drip water; (2) identify the influence of vegetation restoration on the interannual variations in stable isotopes values and elements/ions concentrations of drip water; (3) determine whether the stable isotopes values and elements/ions concentrations of drip waters also reflect variations in vegetation.

## 2. Site description

### 2.1. Background

This study was conducted at the Puding Karst Ecosystem Research Station Chinese Academy of Sciences (hereafter referred to as Puding Station), in Puding County, Guizhou Province, southwest China (Fig. 1a). Shawan Cave (26.36°N, 105.76°E; 1170 m above sea level) is developed in the pure and thick limestone of the Middle Triassic ($T_2g$) Guangling Formation. The whole depth of the soil profile overlying the cave is about 50 cm. This region is characterized by a typical subtropical monsoonal climate. The mean annual temperature (MAT) in

Puding between 1961 and 2008 was 15.1 °C, and the mean annual precipitation (MAP) was 1315 mm, of which ~80% occurred during the rainy season from April to October (Hu et al., 2018).

### 2.2. Shawan cave

The length of the accessible passage in Shawan Cave is about 30 m, with a width of 3 m and a height of 5 m. The thickness of overlying host rock is about 6–8 m. Five drip sites are located in the main chamber: site 1# is situated below the entrance. Site 2# is located in the middle of the chamber, the distance between the monitoring sites and entrance is 10 m. And sites 3#, 4#, and 5# are at the end of the chamber, the distance between the monitoring sites and entrance is 25 m (Fig. 1b). Each of the five drip sites is associated with a corresponding stalactite tip that feeds a stalagmite. Hydrological data reported elsewhere for the five sites suggests that calcite precipitation occurred more during the spring and summer and less during the autumn and winter (Lyu et al., 2020).

### 2.3. Vegetation

The vegetation of Puding Station recovered naturally from cultivated land (corn and canola) after 2010, and is now considered to be a tree–shrub–grassland ecosystem, where trees, shrubs, grass, and bare land account for approximately 22%, 44%, 8%, and 21% of the total land area, respectively. The canopy height is uneven, whereby the heights of single trees, shrubs, and grass ranges from 4 m to 10 m, 1 m to 2 m, and 0 m to 1 m, respectively (Wang et al., 2020b).

## 3. Materials and methods

### 3.1. Data on meteorology and cave microenvironment

During 2017–2019, the daily air temperature and daily rainfall outside Shawan Cave were continuously recorded every 1 h, at an automatic meteorological station at Puding Station. A HOBO Pro V2 data logger (ONSET Company Inc., USA) was used to measure the cave air temperature and humidity. It was installed at a height of 1 m above the floor in the cave chamber. The data were recorded between 2017 and 2019 every 30 min. The drip rates from the five drip sites were measured using automatic drip loggers (Stalagmate MK3). These drip loggers recorded the amount of drip water every 30 min during 2017–2019. We calculated the drip rate (L/S) by measuring the volume of about 0.1 ml/drip.

### 3.2. Vegetation biomass and breast-height diameter

The vegetation biomass was calculated using Eq. (1) (Liu et al., 2009):

$$W = a(D^2H)^b \quad (1)$$

where $W$ is biomass, $D$ is breast-height diameter, $H$ is height, and $a$ and $b$ are constants. The breast-height diameter and height for all trees and shrubs were measured in 2012 and 2017 in the Shawan plot. The breast-height diameter of a hundred trees in the Shawan plot has been measured using growth rings since April 2018. These trees can be divided into 19 species.

### 3.3. Soil air and cave air data

We chose a soil profile above Shawan Cave and divided it into five separate soil layers for soil-air sampling: S1 (0–10 cm), S2 (10–20 cm), S3 (20–30 cm), S4 (30–40 cm), and S5 (40–50 cm). The soil-air samples were collected every month from April 2018 to December 2019, which was injected into the airbag using a 250 ml syringe. And the sampling time each time is between 8:30 pm and 11:30 pm. 3 soil-air samples were collected in each layer as a total of 15 soil-air samples each month. These samples that were purified and sealed in the glass tube were subsequently measured for $\delta^{13}C$ using a MAT-252 mass spectrometer. The measured values are reported relative to the V-PDB standard with an uncertainty less than ± 0.03‰. A HOBO Pro V2 data logger (ONSET Company Inc., USA) was used to measure the water content of the soil profile. The $P_{CO_2}$ of the soil air and cave air were continuously, automatically measured using a CCIA-DLT-EP $CO_2$ carbon isotope analyzer (Los Gatos Research, USA). The measuring range of $CO_2$ concentration is from 380 to 25000 ppm, and the measuring frequency is 1 Hz. The measurement site for the soil air was at a depth of 50 cm in the soil profile, and the measurement site for the cave air was located in the cave chamber. The carbon isotope analyzer has 8 air inlets. It measures cycle twice every half hour (We only used the data of the measurement site for the cave and soil in this study). Each air inlet was measured 120 s in the first cycle and each air inlet was measured 105 s in the second cycle. The value each air inlet was obtained each half-hour, through getting a mean value of observation value each cycle.

### 3.4. Rainwater and drip water data

Rainfall samples were obtained in the rainy seasons during 2017–2019 (April 21, 2017–October 11, 2017, March 29, 2018–September 28, 2018, and April 4, 2019–November 4, 2019), which were collected by standard gauges for the isotopic measurements. The samples were removed from the collectors and passed through 0.45 μm Millipore filters into brown glass bottles soon after each rainfall event to prevent evaporation. In-situ collection of the drip water samples were also made at the five drip sites every 1–2 weeks from January 2017 to January 2018, and every month from February 2018 to December 2019. The drip water remained in a container for 0.5–2 h in the rainy season and 16–18 h in the dry season since July 2018. Drip water and were filtered through 0.45 μm Millipore filters and then refrigerated (approximately 4 °C) in brown glass bottles awaiting analysis.

Oxygen and hydrogen isotopes of rainwater and drip water samples were measured by a DLT-100 liquid water isotope analyzer (IWA-35EP; Los Gatos Research, USA). The 1σ precision was 0.1‰ for $\delta^{18}O$ and 0.5‰ for $\delta^{2}H$. The isotope data are reported relative to the Vienna-Standard Mean Ocean Water (VSMOW). Rainwater oxygen isotope values of the dry season during 2017–2018 (January 3, 2017–April 6, 2017, October 12, 2017–March 28, 2018, and October 13, 2018–December 25, 2018) were acquired from a study of the Shawan Test Site (Hu et al., 2020). The $\delta^{13}C_{DIC}$ value of drip water samples was analyzed using a MAT-252 mass spectrometer.

Cations were measure using inductively-coupled plasma atomic-emission spectroscopy (ICP–OES) after acidification of the samples with 1% $HNO_3$. Anions were measured using ion chromatography (ICS90). The cation and anion experimental detection resolution was 0.01 mg $L^{-1}$. The $HCO_3^-$ concentration was titrated immediately in the cave using an alkalinity test (Merck KGaA Company, Germany) with an accuracy of 0.1 mmol $L^{-1}$.

### 3.5. Drip water residence time estimation

Mean residence times of drip water in Shawan Cave could be estimated by the seasonal variations of the $\delta^{18}O$ values in drip water and rainfall. The seasonal variations of the $\delta^{18}O$ values follow a generalized equation of the sine function relationship (Reddy et al., 2006):

$$\delta^{18}O = \text{mean}(\delta^{18}O) + A\sin\left[\left(\frac{2\pi x}{b}\right) + c\right] \quad (2)$$

where *mean($\delta^{18}O$)* is the annual mean $\delta^{18}O$ in ‰, $A$ is the seasonal amplitude of $\delta^{18}O$, $b$ is the period of the seasonal cycle, $x$ is time in days, and $c$ is the phase lag in radians.

These parameters could be calculated by a curve-fitting algorithm.

And the residence time of drip water is obtained by Eqs. (3), (4), (5), and (6) below (Hu et al., 2020):

$$\frac{2\pi t_0}{b} + c = \frac{\pi}{2} + 2n\pi \quad (3)$$

$$t = t_0(\text{dripwater}) - t_0(\text{rainfall}) \quad (4)$$

$$-2\pi < c < \frac{\pi}{2} n = 0 \quad (5)$$

$$\frac{\pi}{2} < c < 2\pi n = 1, 2, 3 \quad (6)$$

where $c$ is the phase lag of radians in the fitted sine curve and $t$ the mean residence time of drip water.

### 3.6. Principal components analysis (PCA) on drip water

A PCA of the main anion and cation concentrations of the sampled drip water was performed using SPSS 17.0 software (SPSS Inc., Chicago, IL, USA). This provided a multi-dimensional correlation analysis, whereby the main modes of variability of the normalized data are identified and expressed as the first, second, … nth principal components (PC1, PC2, … PCn) of variation. The loadings of individual parameters on each PC are then used for qualitative comparison (Treble et al., 2016).

## 4. Results

### 4.1. Data on meteorology and cave microenvironment

The daily mean air temperature ranged between −0.3 °C and 28.9 °C (mean value of 16.7 °C) during the monitoring period. The daily rainfall ranged from 0 mm to 102.8 mm. The daily temperature and rainfall were higher between April and October, and lower between November and March of the following year. The annual mean air temperature in 2017, 2018, and 2019 was 17.4 °C, 16.4 °C, and 16.3 °C, respectively, while the annual rainfall in 2017, 2018, and 2019 were 1166 mm, 1408 mm, and 1064 mm, respectively (Fig. 2d). The annual mean value of cave air temperature in 2017, 2018, and 2019 was 17.7 °C, 17.5 °C, and 17.2 °C, respectively (Fig. 2d). The cave relative humidity was always 100% during the study period.

### 4.2. Vegetation variation

The yearly difference of biomass in the Shawan plot was 184.9 g $m^{-2}$ based on vegetation survey in 2012 and 2017. The mean value of the monthly increase in the breast-height diameter was 0.068 cm for the period from April 2018 to April 2019, and 0.072 cm for the period from April 2019 to April 2020. Hence, the monthly mean breast-height diameter exhibited an increasing trend between April 2018 and April 2020 (Fig. 3), which indicates that the vegetation in the Shawan plot gradually recovered over this period.

### 4.3. $P_{CO_2}$, and $\delta^{13}C$ values, and soil water content

The $P_{CO_2}$ of soil air overlying Shawan Cave presented a significant seasonal variation. From April to October in each year, the $P_{CO_2}$ of soil air was relatively higher, whereas it was lower from November to March of the following years. There was a significant interannual change in soil air $P_{CO_2}$. The mean $P_{CO_2}$ of soil air in 2017, 2018, and 2019 was 2780 ppm, 3164 ppm, and 3197 ppm, respectively (Fig. 4c).

There were seasonal and interannual variations in $\delta^{13}C$ values of soil air in the soil profiles. The $\delta^{13}C$ values of soil profiles were more negative during the spring and summer in comparison to those during the autumn and winter. The mean $\delta^{13}C$ value of the soil air in the period from April to December 2018 and from April to December 2019 were −20.65‰ and −20.80‰, respectively. The mean value of soil water content was 36% in the soil profiles from November 2018 to December 2019 (Fig. 5).

The $P_{CO_2}$ value of cave air was lower from April to October each year than that from November to March of the following years. The annual mean $P_{CO_2}$ value of cave air in 2017, 2018, and 2019 was 5468 ppm, 6091 ppm, and 7083 ppm, respectively (Fig. 4b). The $\delta^{13}C_{DIC}$ value of drip water from the five drip sites displayed significant interannual variations. The annual mean $\delta^{13}C_{DIC}$ value of drip water in 2017, 2018, and 2019 was −13.48‰, −13.60‰, and −13.31‰, respectively. The mean $\delta^{13}C_{DIC}$ value of drip water during the autumn and winter in 2017, 2018, and 2019 were −15.20‰, −15.35‰, and −15.57‰, respectively (Fig. 4a); thus, these values decreased year-by-year.

### 4.4. $\delta^{18}O$ and $\delta^{2}H$ values

The oxygen isotope ratio in rainwater samples ranged from −16.4‰ to −1.3‰. The $\delta^{18}O$ value of rainwater exhibited an obvious seasonal variation, whereby the values from April to October were more negative than those from November to March of the following year. The annual amount-weighted mean value of rainwater $\delta^{18}O$ in the rainfall in the year 2017, 2018, and 2019 was −8.3‰, −8.4‰, and −7.8‰, respectively. Based on the $\delta^{18}O$ and $\delta^{2}H$ values of the rainwater samples taken from outside Shawan Cave (Fig. 2b), the equation of the local meteoric water line (LMWL) was determined as $\delta^{2}H = 8.628\delta^{18}O + 16.87$, with a correlation coefficient ($R^2$) of 0.94 (Fig. 6), which was similar to that obtained at the Shawan Test Site.

The $\delta^{18}O$ value of the drip water samples from the five drip sites varied from −10.7‰ to −7.2‰. There was a significant seasonal variation whereby the $\delta^{18}O$ values from April to October were more positive than those from November to March of the following year (Fig. 2a). The annual mean $\delta^{18}O$ value of drip water in 2017, 2018, and 2019 was −9.3‰, −8.9‰, and −8.6‰, respectively.

### 4.5. Drip water residence times

The sine functions form of $\delta^{18}O$ value of the rainfall and five drip sites during the three years were determined as $\delta^{18}O_r = -6.20 + 3.84\sin((2\pi x/359) + 6.10)$ ($R^2 = 0.58$) and $\delta^{18}O_d = -9.03 + 0.76\sin((2\pi x/428) + 4.12)$ ($R^2 = 0.30$), respectively (Fig. 7). According to the relationship between rainfall $\delta^{18}O$ and drip waters $\delta^{18}O$, the mean residence time of drip water was calculated with Eqs. (3), (4), (5), and (6). The mean residence time was 154 days (0.42 years).

### 4.6. Discharge variability of drip waters

The drip rates at all the sites were higher in the rainy season and lower in the dry season. The annual mean drip rate of five drip sites in 2017, 2018, and 2019 was $1.93*10^{-5}$ L/S, $2.63*10^{-5}$ L/S, and $2.32*10^{-4}$ L/S, respectively (Fig. 2c). The hydrological behavior of the drip sites was determined using the maximum discharge and the coefficient of variation (Baldini et al., 2006). The 1#, 2#, 3#, 4#, and 5#, with high drip rate maximum and drip rate variability, were classified as seasonal drips (Fig. 8). The 1# that suggests a threshold response to rainfall amount may be as an overflow drip site (Arbel et al., 2010).

### 4.7. Main element/ion concentrations in drip water

The main elements/ions concentration ranges in drip waters were: $Ca^{2+}$ = 33.74–156.01 mg $L^{-1}$, $Mg^{2+}$ = 6.77–17.98 mg $L^{-1}$, $Na^{+}$ = 0.39–2.86 mg $L^{-1}$, $K^{+}$ = 0.003–8.37 mg $L^{-1}$, $Sr^{2+}$ = 0.001–0.24 mg $L^{-1}$, $Cl^{-}$ = 0.02–13.82 mg $L^{-1}$, $SO_4^{2-}$ = 8.87–28.73 mg $L^{-1}$, and $HCO_3^{-}$ = 2.0–5.8 mmol $L^{-1}$ (Fig. 9). There were interannual variabilities in $Ca^{2+}$, $Mg^{2+}$, $Na^{+}$, $K^{+}$, $SO_4^{2-}$, and $Cl^{-}$ concentrations at all of the drip sites. The annual (2017, 2018, and 2019) mean concentrations of all of these elements/

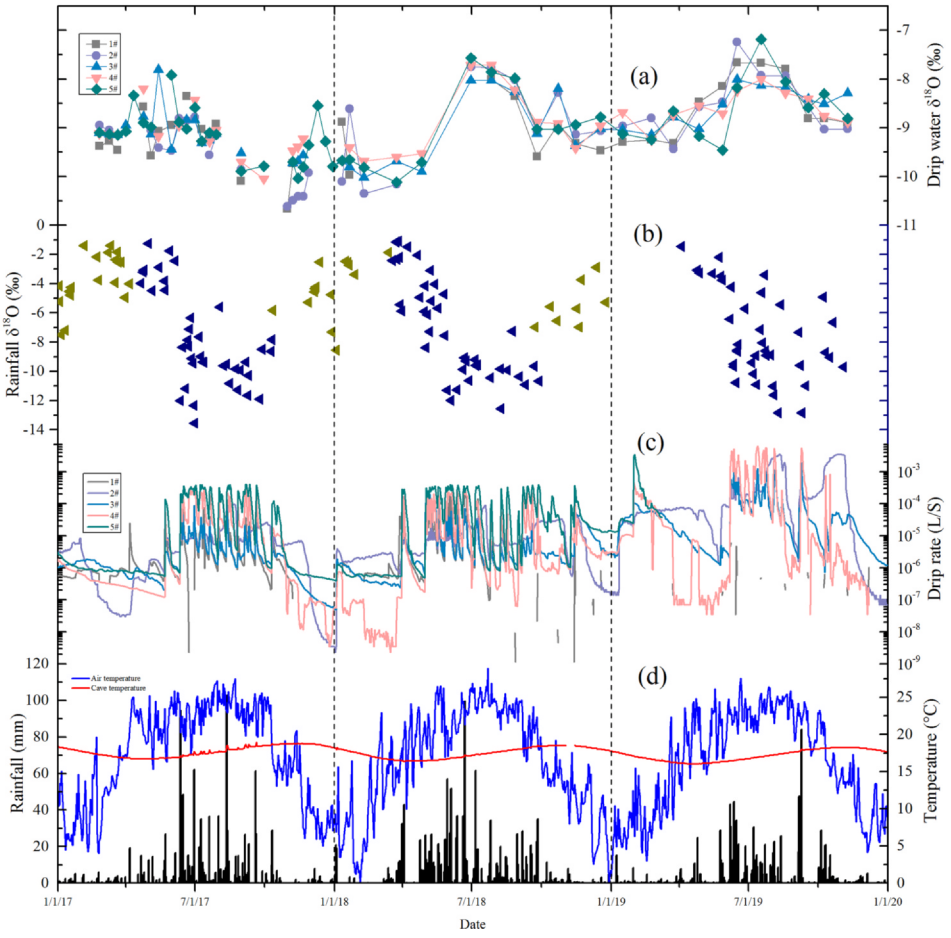


**Fig. 2.** (a) Drip water $\delta^{18}O$ value for the five drip sites, (b) $\delta^{18}O$ value of rainfall, the yellow dots are data from the study of Shawan Test Site (c) drip rate for the five drip sites, and (d) daily mean air temperature, daily mean cave air temperature, and daily rainfall. (For interpretation of the references to colour in this figure legend, the reader is referred to the web version of this article.)

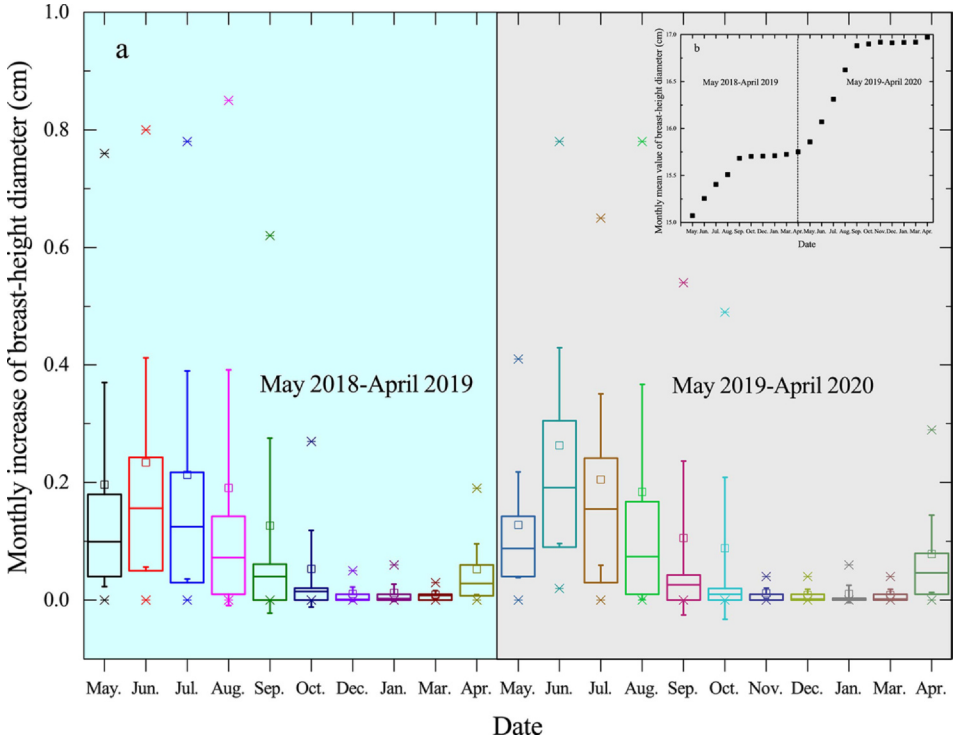


**Fig. 3.** (a) Monthly increase of the breast-height diameter of trees in the Shawan plot. (b) Monthly mean breast-height diameter of trees in the Shawan plot. 'May.': April 13 to May 16, 2018; 'Jun.': May 16 to June 16, 2018; 'Jul.': June 16 to July 13, 2018; 'Aug.': July 13 to August 12, 2018; 'Sep.': August 12 to September 13, 2018; 'Oct.': September 13 to October 15, 2018; 'Dec.': October 15 to December 13, 2018; 'Jan.': December 13, 2018, to January 14, 2019; 'Mar.': January 14 to March 14, 2019; 'Apr.': March 14 to April 13, 2019; 'May.': April 13 to May 13, 2019; 'Jun.': May 13 to June 17, 2019; 'Jul.': June 17 to July 13, 2019; 'Aug.': July 13 to August 14, 2019; 'Sep.': August 14 to September 13, 2019; 'Oct.': September 13 to October 15, 2019; 'Nov.': October 15 to November 13, 2019: 'Dec.': November 13 to December 14, 2019; 'Jan.': December 14, 2019, to January 13, 2020; 'Mar.': January 13 to March 10, 2020; 'Apr.': March 10 and April 12, 2020.

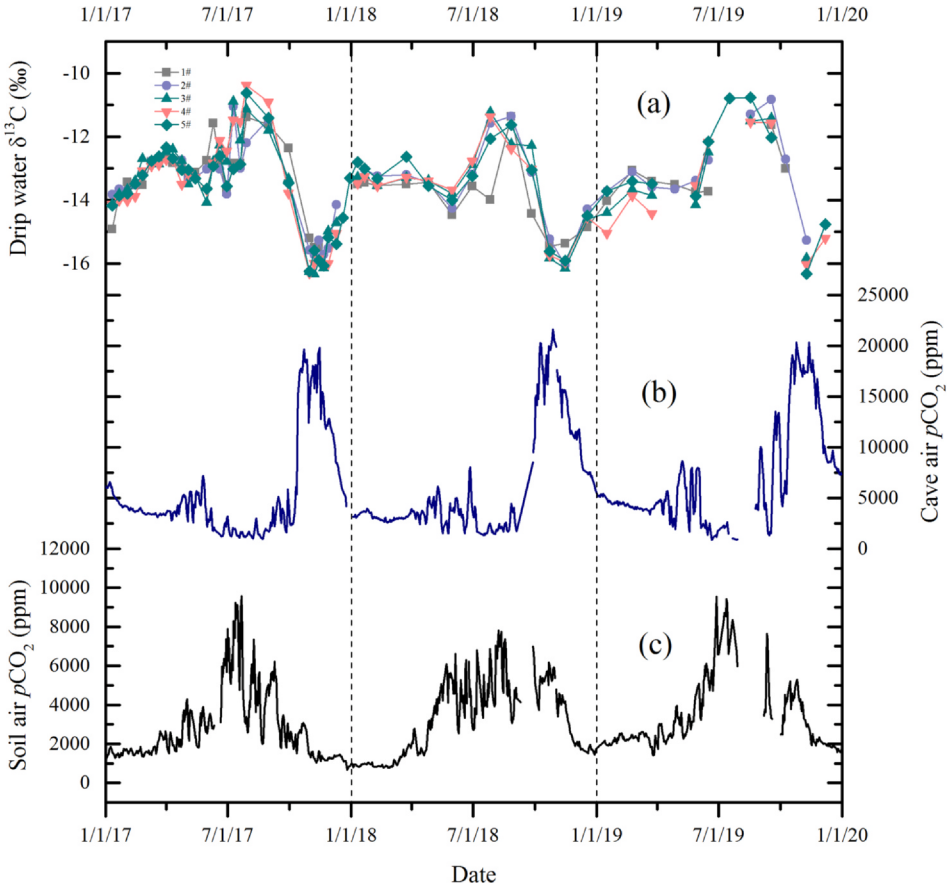


**Fig. 4.** (a) Drip water $\delta^{13}C_{DIC}$ value at the five drip sites, (b) daily mean cave air $P_{CO_2}$, and (c) daily mean soil air $P_{CO_2}$.

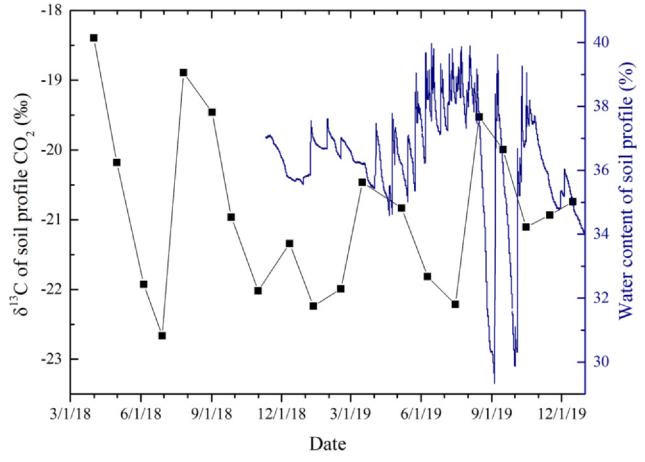


**Fig. 5.** Temporal variations in mean $\delta^{13}C$ value and mean soil water content of the five soil layers in soil profile.

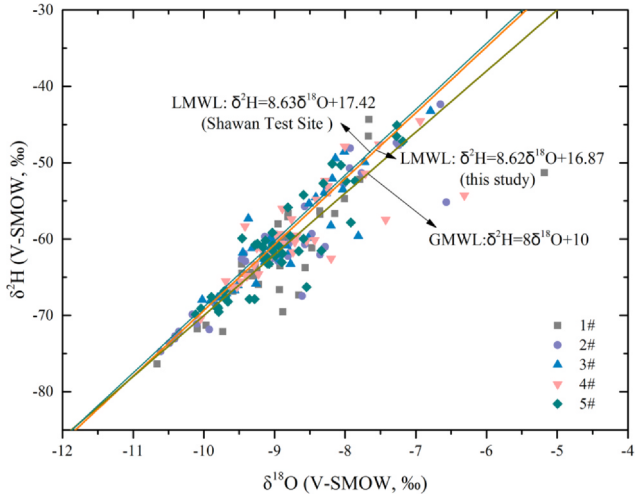


**Fig. 6.** Relationships between the stable isotope compositions at the five drip sites and the LMWLs.

ions presented year-by-year increasing trends, whereas $SO_4^{2-}$ shows the opposite trends (Table 1). There were obvious seasonal variations in the $Sr^{2+}$ and $HCO_3^-$ concentrations at all five drip sites, with higher values during the winter and spring in comparison to the summer and autumn (Fig. 9e and f), although the interannual variations were insignificant. The Mg/Ca ratio and 1000 × Sr/Ca value ranged from 0.06 to 0.36 (mean of 0.18) and 0.0009–0.42 (mean of 0.21), respectively. The five drip sites had no clear seasonal or interannual characteristics (Fig. 9a and b). The lower Mg/Ca and 1000 × Sr/Ca values of drip waters indicate that there was less prior calcite precipitation (PCP) in the carbonate matrix and cave ceiling (Dhungana and Aharon, 2019; Mattey et al., 2010)

## 5. Discussion

### 5.1. Lag times of drip water isotopic signature and its response to vegetation restoration

Generally, the lag time of drip water from the surface to a cave is highly variable and ranges from several days to several years (Riechelmann et al., 2017); hence, studies of various caves have

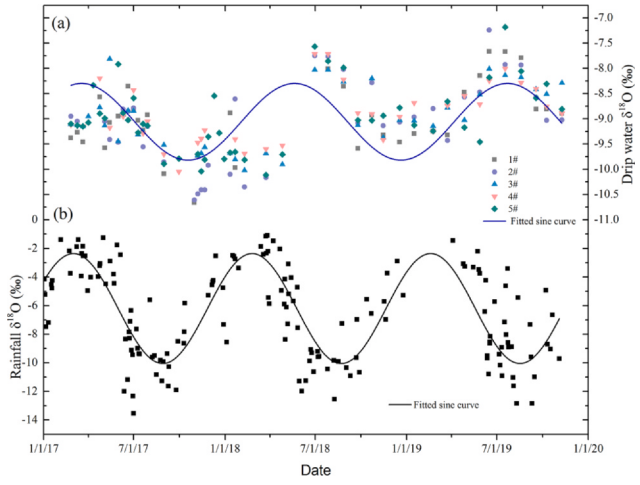


**Fig. 7.** The fitted sine curves $\delta^{18}O$ in rainfall and drip waters during 2017–2019. (a) and (b) are drip waters $\delta^{18}O$ and rainfall $\delta^{18}O$, respectively.

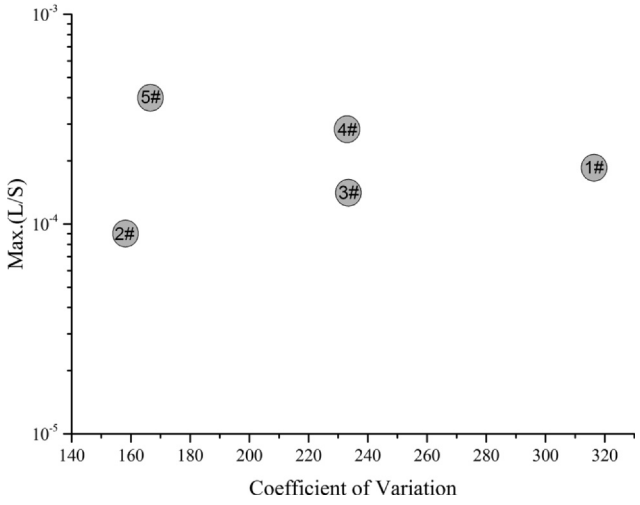


**Fig. 8.** Hydrological behavior of the five drip sites (1#, 2#, 3#, 4#, and 5#) determined in terms of maximum discharge versus coefficient of variation in discharge.

observed different lag times. Moreover, the lag times of different drip sites within the same cave can also vary (Luo et al., 2014; Moerman et al., 2014; Pérez-Mejías et al., 2018; Treble et al., 2013). Some studies have reported that the $\delta^{18}O$ value of drip water retains some of the seasonality of the $\delta^{18}O$ value of rainfall, which leads to a significant seasonal variation in the $\delta^{18}O$ value of drip water (Beynen and Febbroriello, 2005; Cobb et al., 2007; Fuller et al., 2008). This results in short lag times of several days or several months. Some studies have proposed that an attenuated seasonal variation in the $\delta^{18}O$ value of drip water was observed during their monitoring, which could have been influenced by the mixing effect of old and fresh waters (Genty et al., 2014; Luo and Wang, 2008; Riechelmann et al., 2011; Yonge et al., 1985). Thus this results in long lag times of several years. In this study, the $\delta^{18}O$ value of drip water at each site exhibited an obvious seasonal variation, which was opposite to the seasonal variation in the $\delta^{18}O$ value of rainfall. Here, we first rule out that there is an evaporation effect in drip water inside the cave, based on almost constant cave air temperature and always 100% of cave relative humidity during the study period. The mean residence time of drip waters was 154 days (0.42 years) through the calculation. On the basis of the change in the water excess, which serves as an indicator of the amount of infiltration, the water in the aquifer was in excess during the spring and summer and was deficit during the autumn and winter because there was more rainfall during the spring and summer (Kelley et al., 2019). This may have caused the inundation of heavy rainfall to the cave during the spring and summer, which effectively flushed out the water that had accumulated in the epikarst during the autumn and winter. This would have led to higher $\delta^{18}O$ values in the drip water during the spring and summer seasons in comparison to the autumn and winter. This would also explain the observed opposite correlations between the $\delta^{18}O$ values of drip water and rainfall during the study period.

The annual mean $\delta^{18}O$ values of drip water displayed a year-by-year increasing trend. Based on the fact that the lag time of drip water relative to rainfall was 154 days. The annual mean $\delta^{18}O$ value of drip water was −9.08‰, −8.77‰, and −8.53‰ for September 2016 to August 2017, September 2017 to August 2018, and September 2018 to June 2019, respectively; hence, there also was a gradually increasing trend over these years. Most studies have found that the amount of rainfall and the $\delta^{18}O$ value of rainfall are the main factors influencing the $\delta^{18}O$ value of drip water (Breitenbach et al., 2015; Cobb et al., 2007; Duan et al., 2016). However, the annual rainfall amount and the amount-weighted mean value of rainwater $\delta^{18}O$ did not show a yearly increase or decrease in our study. If the only variables influencing the $\delta^{18}O$ value of drip water are the amount-weighted mean value of rainwater $\delta^{18}O$ and the rainfall amount, there would not have been a year-by-year increasing annual mean $\delta^{18}O$ values of drip water. This implies that the $\delta^{18}O$ value of drip water may have been affected by other factors, for example, the variation in vegetation. The amounts of evaporation decreased and amounts of transpiration increased from bare soil land to shrub land in Shawan Test (Hu et al., 2018). The ratios of transpiration and evaporation could gradually increase and decrease, respectively, as vegetation flourishes. The transpiration of groundwater increase with groundwater table depth decreases (from a deeper level to 1.5 m) (Wang et al., 2020a). This might have caused the $\delta^{18}O$ value of groundwater to be higher. The vegetation in the Shawan plot gradually recovered year-by-year, and it is likely that the annual mean $\delta^{18}O$ value of drip water decreased year-by-year as the amounts of flourishing vegetation and transpiration increased.

Furthermore, most of the drip water samples were distributed around the LMWL, which suggests that drip water preserved the isotopic signal of rainfall. However, some drip water samples did deviate towards the right of the LMWL, which indicates that these drip water may have experienced evaporative before entering the cave. The three points that deviate the most towards the right of the LMWL were at site 1# on June 10, 2017, site 4# on June 20, 2017, and site 2# on July 10, 2017 (Fig. 10). Hence, there may have been more intense evaporation of drip water during the early stages of this study. According to Fig. 10, the slopes of the evaporation line for the five drip sites in 2017, 2018, and 2019 were 6.29, 7.94, and 8.58, respectively. The year-by-year increasing trend of slopes over these years suggests that the effect of evaporation occurring outside the Shawan Cave on drip water may have experienced a year-by-year decreasing trend over the same period. That is, the drip water, one has not yet entered the cave, experience less evaporation as vegetation restoration. Hence, it is possible that vegetation restoration may have also influenced the variation in the $\delta^{18}O$ value of drip water in Shawan Cave. In summary, variations in vegetation may have influenced the change in the $\delta^{18}O$ value of drip water, whereby vegetation improved, strong transpiration, and weak evaporation resulted in the annual mean $\delta^{18}O$ value of drip water being more positive, and vice versa. The behavior was observed previously in a study undertaken at the Shawan Test Site, whereby evaporation decreased and transpiration increased as vegetation flourished, which led to a change in $\delta^{18}O$ value of seepage water (Hu et al., 2018).

In addition, a year-by-year decreasing trend in annual mean air temperature over the study period agreed with the year-by-year increasing trend in the annual mean $\delta^{18}O$ values of drip water. Usually, high temperatures could promote soil respiration (Curiel Yuste et al., 2010). But a long-term high air temperature may cause a decrease in the soil moisture content, which may limit soil respiration. (Atkin et al.,

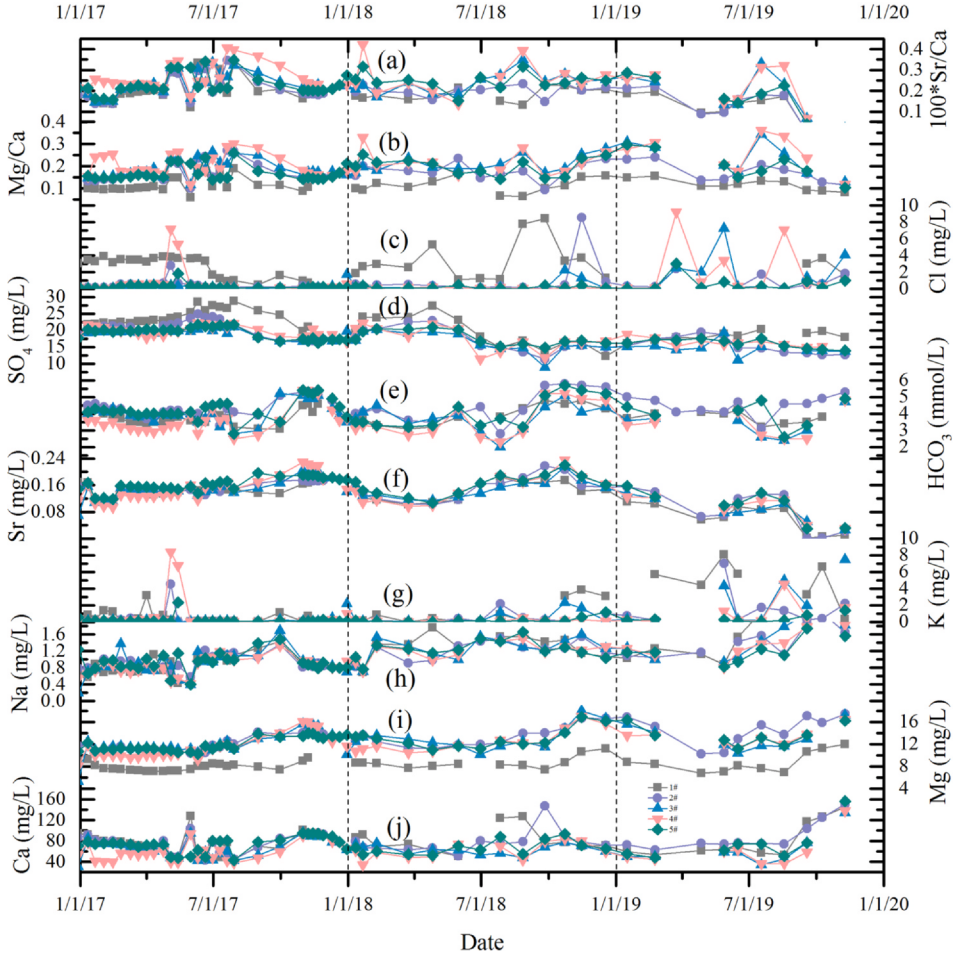


**Fig. 9.** Change characteristic of the hydrogeochemistry at the five drip sites, showing (a) drip water 1000 × Sr/Ca, (b) drip water Mg/Ca, (c–j) $Cl^-$, $SO_4^{2-}$, $HCO_3-$, $Sr^{2+}$, $K^+$, $Na^+$, $Mg^{2+}$, and $Ca^{2+}$ concentrations at the five drip sites in Shawan Cave.

**Table 1**
Annual mean $Ca^{2+}$, $Mg^{2+}$, $Na^+$, $K^+$, $Sr^{2+}$, $SO_4^{2-}$, $Cl^-$, and $HCO_3-$ concentrations.

| Elements/ions Concentrations | $Ca^{2+}$ (mg/L) | SD (σ) | $Mg^{2+}$ (mg/L) | SD (σ) | $Na^+$ (mg/L) | SD (σ) | $K^+$ (mg/L) | SD (σ) | $Sr^{2+}$ (mg/L) | SD (σ) | $SO_4^{2-}$ (mg/L) | SD (σ) | $Cl^-$ (mg/L) | SD (σ) | $HCO_3^-$ (mmol/L) | SD (σ) |
|---|---|---|---|---|---|---|---|---|---|---|---|---|---|---|---|---|
| Annual mean, 2017 | 69.35 | 18.35 | 11.13 | 2.15 | 0.90 | 0.22 | 0.37 | 1.08 | 0.15 | 0.03 | 20.58 | 2.59 | 0.86 | 1.30 | 4.0 | 0.66 |
| Annual mean, 2018 | 70.31 | 19.63 | 12.17 | 2.47 | 1.23 | 0.25 | 0.48 | 0.82 | 0.15 | 0.03 | 17.64 | 3.65 | 1.01 | 1.89 | 4.0 | 0.90 |
| Annual mean, 2018 | 73.45 | 33.54 | 12.65 | 2.90 | 1.43 | 0.45 | 2.08 | 2.43 | 0.08 | 0.04 | 16.14 | 2.10 | 1.65 | 3.05 | 3.8 | 0.79 |

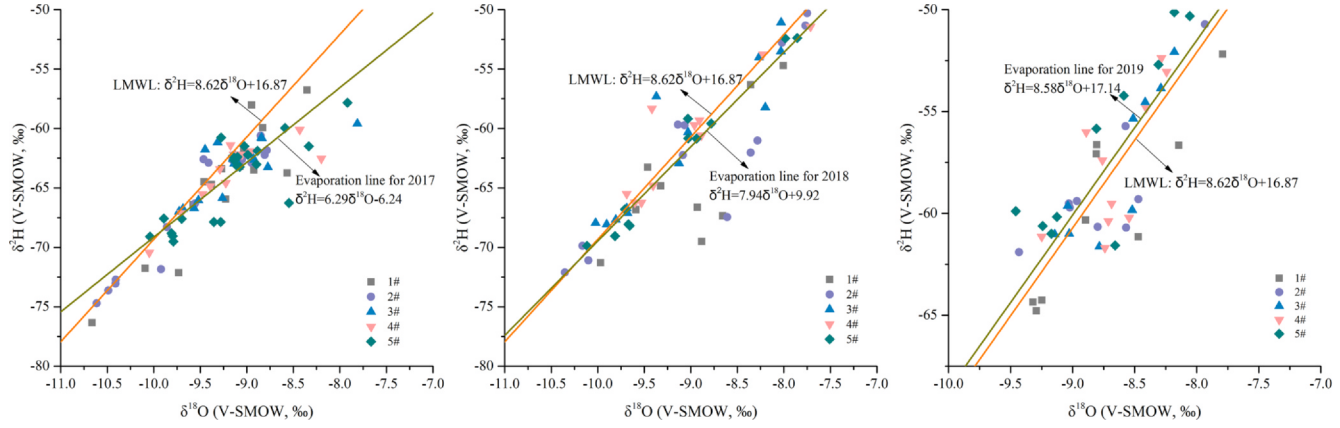


**Fig. 10.** Interannual relationships between the evaporation lines at the five drip sites and the LMWL.

2000). However, the mean air temperature in 2017 was significantly higher than that in 2018 and 2019, and the mean air temperatures between 2018 and 2019 were similar. It is possible that the soil moisture content above Shawan Cave in 2017 was comparatively lower, whereas the soil moisture content of 2018 and 2019 may be a moderate condition. The moderate soil moisture content and air temperature in 2018 and 2019 could have promoted soil respiration, whereas low soil moisture content and high air temperature in 2017 would have limited soil respiration (Cao et al., 2020). Accordingly, soil respiration in 2017 may have been weaker than that in 2018 and 2019. Soil respiration is closely related to variations in vegetation; hence, the change in the air temperature influences the variation in vegetation, which might lead to the variation in the $\delta^{18}O$ value of drip water. Therefore, changes in vegetation may be another potential factor influencing the interannual variation of the $\delta^{18}O$ value of drip water.

### 5.2. Response of drip water $\delta^{13}C_{DIC}$ to vegetation restoration

In karst cave systems, carbon is transported by the interactions between atmospheric $CO_2$, vegetation carbon, soil air $CO_2$, soil water dissolved inorganic carbon (DIC), and drip water DIC (Li et al., 2012, 2018). Soil air $CO_2$ (Dreybrodt and Scholz, 2011; Meyer et al., 2014), bedrock dissolution (Genty et al., 2001), PCP (Bergel et al., 2017; Wong et al., 2011), and cave ventilation (Baldini et al., 2008; Lambert and Aharon, 2011; Spötl et al., 2005) can all affect the $\delta^{13}C_{DIC}$ value of drip water. However, the most important factor that determines the $\delta^{13}C_{DIC}$ value of drip water is the $CO_2$ concentration in soil air (Li et al., 2012). Most studies have indicated that the $\delta^{13}C_{DIC}$ value of drip water is primarily derived from soil air $CO_2$ and host rock dissolution (Frisia et al., 2011; Lambert and Aharon, 2011; Meyer et al., 2014). A previous study undertaken at Shawan Cave found that 3.80% of the DIC in drip water was, on average, dead carbon (Lyu et al., 2020). This suggests that a lower proportion of the $\delta^{13}C_{DIC}$ value of drip water is derived from host rock carbonate dissolution in Shawan Cave, and that the main carbon source is soil-air $CO_2$. As soil-air $CO_2$ is primarily derived from vegetation root respiration, microbial respiration, and the decomposition of organic matter (Mattey et al., 2016), the carbon sources of drip water are almost all related to vegetation. Thus, the $\delta^{13}C_{DIC}$ value of drip water may respond to vegetation change; however, how vegetation restoration induces this change needs to be clarified.

It was found that the vegetation biomass and $CO_2$ concentration of soil air overlying Shawan Cave increased year-by-year. Further, the mean $\delta^{13}C$ value of the soil profile was lower in 2019 in comparison to 2018. Based on the study on the positive correlation of diffusion on soil moisture (Wang et al., 2005), higher the soil water content overlying Shawan Cave could help to accelerate the downward diffusion of $CO_2$. As vegetation flourishes, the vegetation improved and leads to increased root respiration and increased microbial activity. $CO_2$ released under the action of soil moisture diffuses to the soil zone. Thus, the consequential higher production of soil-air $CO_2$ causes the $\delta^{13}C$ value of soil air to be more negative. In general, soil air can enter caves through fissures and soil water also can enter caves as drip water. As the carbon of deeply rooted vegetation is more easily transported to drip water through soil-air $CO_2$ (Breecker et al., 2012; Hao et al., 2019; Meyer et al., 2014), the $\delta^{13}C_{DIC}$ signal of drip water should mirror vegetation changes. However, the $\delta^{13}C$ values of soil air during the autumn and winter were higher than those during the spring and summer, and the $\delta^{13}C_{DIC}$ values of drip water during the autumn and winter were lower than those during the spring and summer. This does not seem to prove that the $\delta^{13}C_{DIC}$ value of drip water reflects the vegetation changes. As mentioned in Section 5.1, the lag time of drip water in this study was estimated to be 154 days. Accordingly, it can be inferred that the $\delta^{13}C_{DIC}$ value of drip water during the autumn and winter can reflect the vegetation signal of the previous spring and summer. With respect to the cave air, the lag time of the $CO_2$ concentration in the cave air was also ~5 months relative to the $CO_2$ concentration in the soil air (Fig. 4b and c). Here, we first exclude the effect of degassing of drip water on $CO_2$ concentration in the cave air. Because the five drip sites were seasonal drips, the degassing of drip water was more in the rainy season, but $CO_2$ concentration in the cave air was lower during the same period. This suggests the degassing of drip water may be not the main cause of the changes in $CO_2$ concentration in cave air. Hence this behavior may have been caused by cave ventilation (Lyu et al., 2020). That is, stagnation of the cave air during the autumn and winter increased the $P_{CO_2}$ of the cave air, which led to a decrease in the $\delta^{13}C_{DIC}$ value of drip water. Thus, the $\delta^{13}C_{DIC}$ value of drip water during the autumn and winter could provide a better indication of the vegetation change during the previous spring and summer. This is because a high $P_{CO_2}$ in cave air is the result of the accumulation of $CO_2$ in soil air during the autumn and winter seasons under stagnated cave air (The large difference of $CO_2$ concentration between cave air and soil air may be ascribed to the cave ventilation. The air of Shawan Cave rarely exchanges with the atmosphere in the autumn and winter seasons, leading to cave air stagnation. The cave air that come from soil air accumulates at the bottom of the cave, which causes that $CO_2$ concentration of cave air is much higher than those of soil air.).

The annual mean $\delta^{13}C_{DIC}$ value of drip water in 2018 was lower than that in 2017. It can be implied that the $\delta^{13}C_{DIC}$ value of drip water may have responded to vegetation restoration through the influence of vegetation restoration to changes in the $CO_2$ concentration and $\delta^{13}C$ value of soil air. However, the annual mean $\delta^{13}C_{DIC}$ value of drip water was higher in 2019 than that in 2017. It is possible that lower annual rainfall (1064 mm in 2019 versus 1166 mm in 2017 and 1408 mm in 2018) reduced the flux of $CO_2$ from soil air to drip water and led to the higher annual mean $\delta^{13}C_{DIC}$ value of drip water in 2019. However, the mean $\delta^{13}C_{DIC}$ values of drip water during the autumn and winter decreased year-by-year (Fig. 4a). Moreover, in terms of the interannual variation, the $\delta^{13}C_{DIC}$ values of drip water during the autumn and winter should correspond to the $\delta^{13}C_{DIC}$ value of the previous spring and summer based on the lag time of drip water. As the mean $\delta^{13}C_{DIC}$ values of drip water during the autumn and winter is hardly affected by the exchange of cave air (Lyu et al., 2020), and rainfall in 2017, 2018, and 2019 almost is less during the autumn and winter, the impacts of rainfall and cave ventilation on $\delta^{13}C_{DIC}$ values of drip water could be eliminated to a certain extent. The mean $\delta^{13}C_{DIC}$ values of drip water during the autumn and winter could better reflect vegetation change. Hence, the interannual change in the $\delta^{13}C_{DIC}$ value of drip water could respond to the vegetation restoration process. This behavior has been observed in the studies of the Shawan Test Site (Chen et al., 2017) and the Inner Space Cavern in Texas (Meyer et al., 2014). These studies found that the more flourishing vegetation is, the lower the $\delta^{13}C_{DIC}$ value of drip water is. This further confirms that the change in the $\delta^{13}C_{DIC}$ value of drip water could reflect the vegetation restoration process.

### 5.3. Response of drip water elements to vegetation restoration

It is well understood that the elemental composition of drip water may be derived from rainfall, dust, and soil/bedrock leaching (Baker et al., 2000; Fairchild and Treble, 2009). Usually, the elements/ions concentrations in drip water are primarily dominated by water–rock interactions occurring along seepage-water flow paths, which are associated with the local hydrological characteristics (McDonald and Drysdale, 2007; Tooth and Fairchild, 2003). However, the elements/ions within drip water are largely utilized by vegetation (Wallacke et al., 1979), which may make them more sensitive to biogeochemical processes (Treble et al., 2003). Vegetation can influence the elements/ions concentrations of drip water in two ways. One way involves the organic acids decomposed by vegetation and the subsequent low pH micro-environment around the roots. This can lead to increased weathering rates, which accelerate the release of elements/ions contained within rock and soil, thereby encouraging the exchange of

**Table 2**
Results of a PCA of the entire dataset. The numbers indicate either positive or negative loadings (analogous to a correlation coefficient) of each principal component (PC) for each drip water site. The bottom row gives the total percentage of variation in the data explained by each component.

| | Site 1# | | | Site 2# | | | Site 3# | | | Site 4# | | | Site 5# | | |
|---|---|---|---|---|---|---|---|---|---|---|---|---|---|---|---|
| Element/ion | PC1 | PC2 | PC3 | PC1 | PC2 | PC3 | PC1 | PC2 | PC3 | PC1 | PC2 | PC3 | PC1 | PC2 | PC3 |
| $Ca^{2+}$ | 0.43 | 0.42 | −0.35 | 0.75 | 0.05 | 0.15 | 0.71 | 0.46 | 0.31 | 0.83 | 0.17 | 0.26 | 0.64 | 0.38 | 0.16 |
| $Mg^{2+}$ | 0.62 | 0.31 | −0.45 | 0.89 | 0.01 | 0.02 | 0.67 | 0.42 | −0.37 | 0.83 | 0.22 | −0.27 | 0.72 | 0.39 | −0.21 |
| $Na^{+}$ | 0.52 | −0.34 | −0.56 | 0.66 | 0.04 | −0.65 | 0.56 | −0.46 | −0.50 | 0.31 | −0.25 | −0.86 | 0.50 | −0.34 | −0.62 |
| $K^{+}$ | 0.80 | −0.37 | 0.31 | −0.06 | 0.77 | 0.48 | 0.90 | −0.26 | 0.27 | −0.51 | 0.84 | −0.09 | 0.65 | −0.55 | 0.35 |
| $Sr^{2+}$ | −0.51 | 0.71 | 0.24 | −0.16 | −0.61 | 0.53 | −0.24 | 0.76 | −0.35 | 0.37 | 0.35 | 0.25 | −0.19 | 0.71 | 0.13 |
| $SO_4^{2-}$ | −0.75 | −0.36 | −0.16 | −0.90 | −0.06 | −0.11 | −0.51 | 0.19 | 0.66 | −0.51 | −0.23 | 0.76 | −0.74 | −0.19 | 0.41 |
| $HCO_3^{-}$ | 0.51 | 0.66 | 0.41 | 0.68 | −0.34 | 0.43 | 0.41 | −0.34 | 0.43 | 0.81 | 0.31 | 0.30 | 0.47 | 0.67 | 0.48 |
| $Cl^{-}$ | 0.36 | −0.40 | 0.72 | 0.08 | 0.75 | 0.14 | 0.86 | 0.81 | 0.07 | −0.52 | 0.82 | −0.15 | 0.49 | −0.62 | 0.52 |
| % explained | 33.37 | 21.84 | 18.79 | 38.78 | 20.54 | 14.63 | 41.01 | 24.40 | 15.26 | 42.63 | 22.40 | 20.31 | 32.97 | 25.99 | 16.08 |

elements/ions. Another way is the action of biomass as a nutrient sink and the export of chemical species contained in organic matter to drip water (Calmels et al., 2011; Dean et al., 2014; Edwards and Webb, 2009; Velbel and Price, 2007). In this study, through PCA analysis, three PC are extracted for each drip site. This suggest at least three main processes influence the drip water elements/ions in the Shawan Cave.

A PCA was performed for the time series of each drip site using eight elements/ions: $Ca^{2+}$, $Mg^{2+}$, $Na^{+}$, $K^{+}$, $Sr^{2+}$, $SO_4^{2-}$, $HCO_3^{-}$, and $Cl^{-}$. Three PCs (PC1, PC2, and PC3) of sites 1#, 2#, 3#, 4#, and 5# explained approximately 74.00%, 73.95%, 80.67%, 85.34%, and 75.04% of the total variance, respectively. The loadings of each parameter are provided in Table 2, which shows that $Ca^{2+}$, $Mg^{2+}$, $Na^{+}$, and $HCO_3^{-}$ at all drip sites and $K^{+}$ at sites 1#, 3#, and 5# were positive in PC1, whilst $SO_4^{2-}$ and $Sr^{2+}$ (except site 4#) were negative. Drip waters $SO_4^{2-}$ of caves where the soil is thin and vegetation cover is scarce could reflect atmospheric source (Wynn et al., 2012). Because vegetation overlying Shawan Cave is flourishing, drip waters $SO_4^{2-}$ may not reflect the atmospheric source. The negative loading of $SO_4^{2-}$ suggests a greater removal of $SO_4^{2-}$ from drip water, which may then be taken up by vegetation (Borsato et al., 2015; Dean et al., 2014). The same mechanism can be inferred from a year-by-year decreasing trend of $SO_4^{2-}$ concentrations. The overburden media (e.g., vegetation) above the cave have a certain adsorption effect on the $SO_4^{2-}$ contained in drip water that flows through the soil and rock layers (Yang et al., 2012). As vegetation gradually recovered, the $SO_4^{2-}$ concentration gradually decreased in the drip water of Shawan Cave. Although the loadings of $Sr^{2+}$ at sites 1#, 2#, 3#, and 5# were negative in PC1, the absolute values were comparatively small. Because the drip water residence time is 154 days dominated by rainfall in the epikarst and $Sr^{2+}$ is a trace element that originates from rock (Wong et al., 2011). It can be inferred the water–rock interaction process can have been relatively strong. The origin of $Ca^{2+}$, $Mg^{2+}$, $Na^{+}$, and $K^{+}$ is the soil and bedrock in the carbonate area (Zhou and Wang, 2005), and the concentrations of these elements should be high under strong water–rock interactions, because the water in the epikarst is constantly dissolving the bedrock. This may lead to the positive loadings of $Ca^{2+}$, $Mg^{2+}$, $Na^{+}$, and $K^{+}$ in PC1. The $Sr^{2+}$ positive loadings for sites 1#, 3#, 4#, and 5# in PC2 were relatively large, which further confirms strong water–rock interactions. The positive loadings of $K^{+}$ for sites 2# and 4# in PC2 were also comparatively large; hence, the $K^{+}$ concentrations at these sites were high under strong water–rock interactions. Positive loadings of $Cl^{-}$ in PC2 and PC3 were determined for sites 2#, 3#, and 4#, and sites 1# and 5#, respectively. The $Cl^{-}$ concentration is known to be controlled by the transpiration effect, whereby a higher $Cl^{-}$ concentration results from increased transpiration (Treble et al., 2016). The positive loadings of $Cl^{-}$ in PC2 and PC3 indicate that the transpiration effect might have been strong at these drip sites, which implies a considerable influence of vegetation transpiration to these drip sites.

In summary, the PCA identified three main processes that affect the variation in the elements/ions concentrations of drip water in Shawan Cave: 1) vegetation uptake, which indicates how the vegetation influences the chemistry of drip water as it infiltrates through the root zone (Edwards and Webb, 2009); 2) transpiration, which, when strong, implies undergrowth or tree maturation (Treble et al., 2016); 3) water–-rock interactions, which, when strong, suggest a relatively high dissolution of the host rock. It was found that the concentrations of $Ca^{2+}$, $Mg^{2+}$, $Na^{+}$, $K^{+}$, and $Cl^{-}$ in drip water increased year-by-year over the study period, whereas the $SO_4^{2-}$ concentration decreased (Fig. 7). These variations might be attributed to the vegetation recovery above Shawan Cave; thus, variations in the vegetation mainly affected the changes in the elements/ions concentrations of the drip water from three aspects. On the one hand, the $SO_4^{2-}$ ion is taken up by vegetation increased with the flourishing of vegetation, and thereby decreased the $SO_4^{2-}$ concentration in drip water over time. On the other hand, with an increase in flourishing vegetation, there was an increase in organic acids due to the decomposition of vegetation, and the resultant low pH around the roots led to increased weathering rates (Dean et al., 2014; Estrade et al., 2015). This, combined with strong water–rock interactions, accelerated the release of elements from the soil and host rock minerals, and in turn led to increasing trends in the $Ca^{2+}$, $Mg^{2+}$, $Na^{+}$, and $K^{+}$ concentrations of drip water over time. In addition, as the vegetation gradually recovered, the transpiration effect strengthened and caused the $Cl^{-}$ concentration to increase year-by-year. Therefore, the interannual variability in the elements/ions concentrations of drip water was probably influenced by vegetation restoration.

### 5.4. Implications for proxy records of speleothems

The interpretations of the temporal trends in the $\delta^{13}C_{DIC}$ value, $\delta^{18}O$ value, and elements/ions concentrations of drip water suggest that these parameters could have responded to natural vegetation restoration during the monitoring period; hence, these parameters may act as proxies for vegetation change. Numerous studies have indicated that proxies of speleothems offer the opportunity to reconstruct past climate change (Casteel and Banner, 2015; Fairchild and Treble, 2009; Jo et al., 2011; Li et al., 2011; Mattey et al., 2008). In general, proxies of speleothems are associated with regional hydrological change. Regional hydrological change is controlled by temperatures, rainfall, and soil-air $CO_2$ of a region, which can all influence variations in vegetation (Meyer et al., 2014; Sun et al., 2018). For example, southwest China (low latitudes) is located on the main atmospheric moisture transportation pathway and is mainly affected by the Indian Summer monsoon. A strong summer monsoon would cause climate change. And temperature, evaporation, and rainfall could determine effective humidity, which dominated the regional hydrological conditions. Finally, this has a profound effect on variations in vegetation (Kuo et al., 2011; Woo et al., 2015; Wu et al., 2020). Proxies of speleothems may be also related to variations in vegetation. For instance, a study reported that vegetation cover is an important driver of the $\delta^{13}C$ values in speleothems, and that temperature and rainfall are secondary factors in

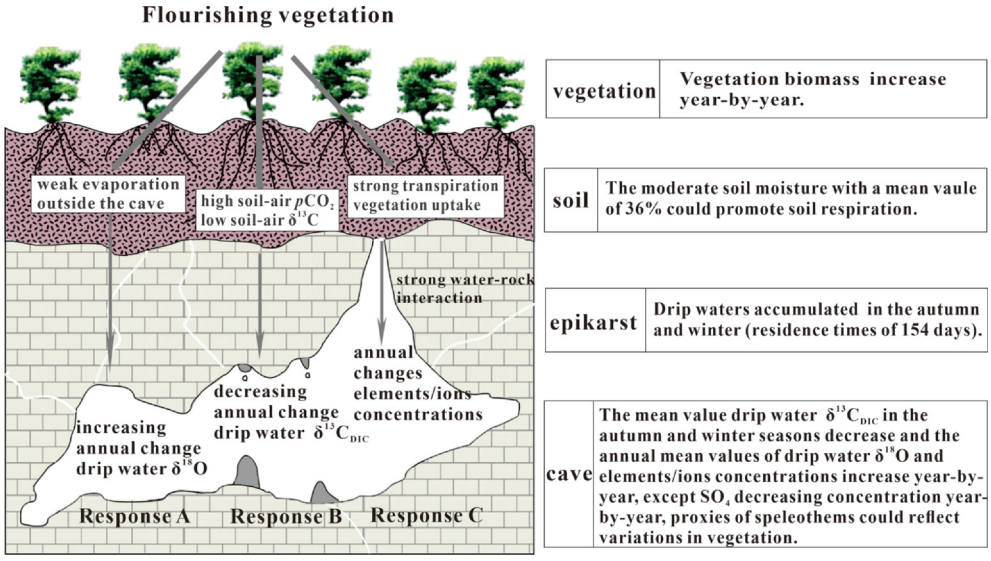


**Fig. 11.** Conceptual model of the geochemical proxies of drip water at Shawan Cave in responses A, B, and C.

monsoon areas (Fohlmeister et al., 2020). Therefore, the $\delta^{13}C$, $\delta^{18}O$, and element/ion of speleothems have the potential to reflect variations in vegetation.

In consideration of climate and the results of this study, a simplified conceptual model is proposed for the relationship between the proxies of speleothems and the variation in vegetation at Shawan Cave (Fig. 11). The model consists of responses A, B, and C. In response A, the $\delta^{18}O$ value of speleothems may potentially reflect vegetation restoration, and is dependent on any evaporation and transpiration effects before drip water reaches the cave. The evaporation (transpiration) effect weakens (strengthens) as vegetation improves, which produces the response of the $\delta^{18}O$ value of speleothems to variations in vegetation. In response B, the $CO_2$ concentration ($\delta^{13}C$ value) of soil air increases (decreases) year-by-year as vegetation restoration progresses, which causes an interannual variability in the $\delta^{13}C_{DIC}$ value of drip water (i.e., it decreases year-by-year during the autumn and winter). This demonstrates that the $\delta^{13}C$ value of speleothems could reflect variations in vegetation. In response C, the variations in the elements/ions concentrations of drip water are caused by vegetation uptake, vegetation transpiration, and water–rock interactions. This causes that elements/ions concentrations of drip water could reflect variation in vegetation. Hence, the $SO_4^{2-}$ associated with speleothems can potentially indicate the variations in the vegetation biomass overlying Shawan Cave, whereas the $Cl^-$ concentration of speleothems might reflect the transpiration effect. Therefore, the coupled study of the $\delta^{13}C_{DIC}$ value, $\delta^{18}O$ value, and elements/ions concentrations in drip water could assist in understanding the mechanisms that speleothem proxies reconstruct variations in vegetation.

## 6. Conclusions

The conditions of the surface and cave were monitored at Shawan Cave for three consecutive years. It was found that the $\delta^{18}O$ values of drip water showed both the seasonal and interannual variations. The $\delta^{18}O$ value of drip water to be more positive during the spring and summer in comparison to that during the autumn and winter, which is caused by the mean residence time of drip water (154 days). The evaporation effect weakened and the transpiration effect strengthened outside the cave as vegetation improved, which may cause an interannual variability in the $\delta^{18}O$ value of drip water to exhibit a year-by-year increasing trend. This indicates that changes in vegetation may have been another factor influencing the change in the $\delta^{18}O$ value of drip water. Meanwhile, carbon isotope values and elements/ions concentrations in drip water also exhibited significant interannual variations. It was inferred that vegetation restoration caused the $CO_2$ concentration ($\delta^{13}C$ value) of soil air to increase (decrease), thereby a year-by-year decreasing the $\delta^{13}C_{DIC}$ value of drip water during the autumn and winter simultaneous to the progressive restoration of vegetation. The variations in the elements/ions concentrations of drip water were influenced by vegetation uptake, vegetation transpiration, and water–rock interactions; hence, the interannual variations in the elements/ions concentrations of drip water may have been associated with vegetation restoration. Accordingly, a conceptual model comprising three responses was proposed, which indicated that the three response modes of $\delta^{18}O$ value, $\delta^{13}C_{DIC}$ value, and elements/ions of drip water to variations in vegetation. It should be noted that the potential for $\delta^{18}O$, S, and Cl of speleothem to be used to track variations in vegetation in the Shawan Cave based on the response of drip water chemistry to variations in vegetation. These findings provide new insights of paleoenvironmental reconstruction using proxies of speleothems.

## Declaration of Competing Interest

The authors declare that they have no known competing financial interests or personal relationships that could have appeared to influence the work reported in this paper.

## Acknowledgment

This work was jointly supported by the Strategic Priority Research Program of the Chinese Academy of Sciences (XDB40020200), the National Natural Science Foundation of China (41673121 and 41663015), and the Science and Technology Support Program of Guizhou Province ([2019]2852). We sincerely thank the anonymous reviewers for their valuable comments and suggestions for this manuscript.

## References

Arbel, Y., Greenbaum, N., Lange, J., Inbar, M., 2010. Infiltration processes and flow rates in developed karst vadose zone using tracers in cave drips. Earth Surf. Process. Landforms 35, 1682–1693.

Atkin, O.K., Edwards, E.J., Loveys, B.R., 2000. Response of root respiration to changes in temperature and its relevance to global warming. New Phytologist 147.

Baker, A., Genty, D., Fairchild, I.J., 2000. Hydrological characterisation of stalagmite drip waters at grotte de Villars, Dordogne, by the analysis of inorganic species and

luminescent organic matter. Hydrol. Earth Syst. Sci. 3, 439–449.
Baker, A., Ito, E., Smart, P.L., Mcewan, R.F., 1997. Elevated and variable values of $^{13}C$ in speleothems in a British cave system. Chem. Geol. 136, 263–270.
Baker, A., Smith, C., Jex, C., Fairchild, I., Genty, D., Fuller, L., 2008. Annually laminated speleothems: a review. Int. J. Speleol. 37, 193–206.
Baldini, J., McDermott, F., Baker, A., Baldini, L., Mattey, D., Railsback, L., 2005. Biomass effects on stalagmite growth and isotope ratios: a 20th century analogue from Wiltshire, England. Earth Planet. Sci. Lett. 240, 486–494.
Baldini, J.U.L., McDermott, F., Fairchild, I.J., 2006. Spatial variability in cave drip water hydrochemistry: implications for stalagmite paleoclimate records. Chem. Geol. 235, 390–404.
Baldini, J.U.L., McDermott, F., Hoffmann, D.L., Richards, D.A., Clipson, N., 2008. Very high-frequency and seasonal cave atmosphere $PCO_2$ variability: implications for stalagmite growth and oxygen isotope-based paleoclimate records. Earth Planet. Sci. Lett. 272, 118–129.
Baskaran, M., Krishnamurthy, R.V., 2013. Speleothems as proxy for the carbon isotope composition of atmospheric $CO_2$. Geophys. Res. Lett. 20, 2905–2908.
Benedetti, M.F., Dia, A., Riotte, J., Chabaux, F., Gérard, M., Boulègue, J., Fritz, B., Chauvel, C., Bulourde, M., Déruelle, B., Ildefonse, P., 2003. Chemical weathering of basaltic lava flows undergoing extreme climatic conditions: the water geochemistry record. Chem. Geol. 201, 1–17.
Bergel, S.J., Carlson, P.E., Larson, T.E., Wood, C.T., Johnson, K.R., Banner, J.L., Breecker, D.O., 2017. Constraining the subsoil carbon source to cave-air $CO_2$ and speleothem calcite in central Texas. Geochim. Cosmochim. Acta 217, 112–127.
Beynen, P.V., Febbroriello, P., 2005. Seasonal isotopic variability of precipitation and cave drip water at Indian Oven Cave, New York . Hydrol. Process. 20, 1793–1803.
Borsato, A., Frisia, S., Fairchild, I.J., Somogyi, A., Susini, J., 2007. Trace element distribution in annual stalagmite laminae mapped by micrometer-resolution X-ray fluorescence: implications for incorporation of environmentally significant species. Geochim. Cosmochim. Acta 71, 1494–1512.
Borsato, A., Frisia, S., Wynn, P.M., Fairchild, I.J., Miorandi, R., 2015. Sulphate concentration in cave dripwater and speleothems: long-term trends and overview of its significance as proxy for environmental processes and climate changes. Quat. Sci. Rev. 127, 48–60.
Bourges, F., Genty, D., Perrier, F., Lartiges, B., Regnier, E., Francois, A., Leplat, J., Touron, S., Bousta, F., Massault, M., Delmotte, M., Dumoulin, J.P., Girault, F., Ramonet, M., Chauveau, C., Rodrigues, P., 2020. Hydrogeological control on carbon dioxide input into the atmosphere of the Chauvet-Pont d'Arc cave. Sci. Total Environ. 716, 136844.
Breecker, D.O., Payne, A.E., Quade, J., Banner, J.L., Ball, C.E., Meyer, K.W., Cowan, B.D., 2012. The sources and sinks of $CO_2$ in caves under mixed woodland and grassland vegetation. Geochim. Cosmochim. Acta 96, 230–246.
Breitenbach, S.F.M., Lechleitner, F.A., Meyer, H., Diengdoh, G., Mattey, D., Marwan, N., 2015. Cave ventilation and rainfall signals in dripwater in a monsoonal setting – a monitoring study from NE India. Chem. Geol. 402, 111–124.
Calmels, D., Galy, A., Hovius, N., Bickle, M., West, A.J., Chen, M.-C., Chapman, H., 2011. Contribution of deep groundwater to the weathering budget in a rapidly eroding mountain belt, Taiwan. Earth Planet. Sci. Lett. 303, 48–58.
Cao, M., Jiang, Y., Chen, Y., Fan, J., He, Q., 2020. Variations of soil $CO_2$ concentration and $pCO_2$ in a cave stream on different time scales in subtropical climatic regime. Catena 185.
Casteel, R.C., Banner, J.L., 2015. Temperature-driven seasonal calcite growth and drip water trace element variations in a well-ventilated Texas cave: implications for speleothem paleoclimate studies. Chem. Geol. 392, 43–58.
Cerling, T.E., 1984. The stable isotopic composition of modern soil carbonate and its relationship to climate. Earth Planet. Sci. Lett. 71, 229–240.
Chen, B., Yang, R., Liu, Z., Sun, H., Yan, H., Zeng, Q., Zeng, S., Zeng, C., Zhao, M., 2017. Coupled control of land uses and aquatic biological processes on the diurnal hydrochemical variations in the five ponds at the Shawan Karst Test Site, China: implications for the carbonate weathering-related carbon sink. Chem. Geol. 456, 58–71.
Cobb, K.M., Adkins, J.F., Partin, J.W., Clark, B., 2007. Regional-scale climate influences on temporal variations of rainwater and cave dripwater oxygen isotopes in northern Borneo. Earth Planet. Sci. Lett. 263, 207–220.
Cosford, J., Qing, H., Mattey, D., Eglington, B., Zhang, M., 2009. Climatic and local effects on stalagmite $\delta^{13}C$ values at Lianhua Cave, China. Palaeogeogr. Palaeoclimatol. Palaeoecol. 280, 235–244.
Cosford, J., Qing, H., Yuan, D., Zhang, M., Holmden, C., Patterson, W., Hai, C., 2008. Millennial-scale variability in the Asian monsoon: evidence from oxygen isotope records from stalagmites in southeastern China. Palaeogeogr. Palaeoclimatol. Palaeoecol. 266, 3–12.
Curiel Yuste, J., Baldocchi, D.D., Gershenson, A., Goldstein, A., Misson, L., Wong, S., 2010. Microbial soil respiration and its dependency on carbon inputs, soil temperature and moisture. Global Change Biol.
Dean, J.F., Webb, J.A., Jacobsen, G.E., Chisari, R., Dresel, P.E., 2014. Biomass uptake and fire as controls on groundwater solute evolution on a southeast Australian granite: aboriginal land management hypothesis. Biogeosciences 11, 4099–4114.
Dhungana, R., Aharon, P., 2019. Stable isotopes and trace elements of drip waters at DeSoto Caverns during rainfall-contrasting years. Chem. Geol. 504, 96–104.
Dogramaci, S.S., Herczeg, A.L., 2002. Strontium and carbon isotope constraints on carbonate-solution interactions and inter-aquifer mixing in groundwaters of the semi-arid Murray Basin, Australia. J. Hydrol. 262, 50–67.
Drever, J.I., Smith, C.L., 1978. Cyclic wetting and drying of the soil zone as an influence on the chemistry of ground water in arid terrains. Am. J. Sci. 278, 1448–1454.
Dreybrodt, W., Scholz, D., 2011. Climatic dependence of stable carbon and oxygen isotope signals recorded in speleothems: from soil water to speleothem calcite. Geochim. Cosmochim. Acta 75, 734–752.
Duan, W., Ruan, J., Luo, W., Li, T., Tian, L., Zeng, G., Zhang, D., Bai, Y., Li, J., Tao, T., 2016. The transfer of seasonal isotopic variability between precipitation and drip water at eight caves in the monsoon regions of China. Geochim. Cosmochim. Acta 183, 250–266.
Edwards, M., Webb, J., 2009. The importance of unsaturated zone biogeochemical processes in determining groundwater composition, southeastern Australia. Hydrogeol. J. 17, 1359–1374.
Estrade, N., Cloquet, C., Echevarria, G., Sterckeman, T., Deng, T., Tang, Y., Morel, J.-L., 2015. Weathering and vegetation controls on nickel isotope fractionation in surface ultramafic environments (Albania). Earth Planet. Sci. Lett. 423, 24–35.
Fairchild, I.J., Frisia, S., 2013. Definition of the Anthropocene: a view from the underworld. Geol. Soc. London Spec. Publ. 395, 239–254.
Fairchild, I.J., Smith, C. L., Baker, A., Fuller, L., Spötl, C., Mattey, D., McDermott, F., E.I. M.F., 2006. Modification and preservation of environmental signals in speleothems. Earth-Sci. Rev. 75, 105–153.
Fairchild, I.J., Treble, P.C., 2009. Trace elements in speleothems as recorders of environmental change. Quat. Sci. Rev. 28, 449–468.
Fohlmeister, J., Voarintsoa, N.R.G., Lechleitner, F.A., Boyd, M., Brandtstätter, S., Jacobson, M.J., Oster, J.L., 2020. Main controls on the stable carbon isotope composition of speleothems. Geochim. Cosmochim. Acta 279, 67–87.
Frisia, S., Fairchild, I.J., Fohlmeister, J., Miorandi, R., Spötl, C., Borsato, A., 2011. Carbon mass-balance modelling and carbon isotope exchange processes in dynamic caves. Geochim. Cosmochim. Acta 75, 380–400.
Fuller, L., Baker, A., Fairchild, I.J., Spötl, C., Marca-Bell, A., Rowe, P., Dennis, P.F., 2008. Isotope hydrology of dripwaters in a Scottish cave and implications for stalagmite palaeoclimate research. Hydrol. Earth Syst. Sci.
Genty, D., Baker, A., Massault, M., Proctor, C., Gilmour, M., Pons-Branchu, E., Hamelin, B., 2001. Dead carbon in stalagmites: carbonate bedrock paleodissolution vs. ageing of soil organic matter. implications for $^{13}C$ variations in speleothems. Geochim. Cosmochim. Acta 65, 3443–3457.
Genty, D., Labuhn, I., Hoffmann, G., Danis, P.A., Mestre, O., Bourges, F., Wainer, K., Massault, M., Van Exter, S., Régnier, E., Orengo, P., Falourd, S., Minster, B., 2014. Rainfall and cave water isotopic relationships in two South-France sites. Geochim. Cosmochim. Acta 131, 323–343.
Hao, Z., Gao, Y., Ma, M., Green, S.M., Wang, J., Song, X., Dungait, J.A.J., Johnes, P.J., Xiong, B., Quine, T.A., Sun, X., Wen, X., He, N., 2019. Using $\delta^{13}C$ to reveal the importance of different water transport pathways in two nested karst basins, Southwest China. J. Hydrol. 571, 425–436.
Hartland, A., Fairchild, I.J., Lead, J.R., Borsato, A., Baker, A., Frisia, S., Baalousha, M., 2012. From soil to cave: transport of trace metals by natural organic matter in karst dripwaters. Chem. Geol. 304–305, 68–82.
Hu, Y., Liu, Z., Ford, D., Zhao, M., Bao, Q., Zeng, C., Gong, X., Wei, Y., Cai, X., Chen, J., 2020. Conservation of oxygen and hydrogen seasonal isotopic signals in meteoric precipitation in groundwater: an experimental tank study of the effects of land cover in a summer monsoon climate. Geochim. Cosmochim. Acta.
Hu, Y., Liu, Z., Zhao, M., Zeng, Q., Zeng, C., Chen, B., Chen, C., He, H., Cai, X., Ou, Y., Chen, J., 2018. Using deuterium excess, precipitation and runoff data to determine evaporation and transpiration: a case study from the Shawan Test Site, Puding, Guizhou, China. Geochim. Cosmochim. Acta 242, 21–33.
Jo, K.N., Woo, K.S., Lim, H.S., Cheng, H., Edwards, R.L., Wang, Y., Jiang, X., Kim, R., Lee, J.I., Yoon, H.I., 2011. Holocene and Eemian climatic optima in the Korean Peninsula based on textural and carbon isotopic records from the stalagmite of the Daeya Cave, South Korea. Quat. Sci. Rev. 30, 1218–1231.
Kelley, J., Rowe, H., Springer, G., Gao, Y., 2019. Multi-year cave dripwater frequency and hydrochemical monitoring of three caves in Eastern North America. J. Cave Karst Stud. 81, 188–202.
Kuo, T.S., Liu, Z.Q., Li, H.C., Wan, N.J., Shen, C.C., Ku, T.L., 2011. Climate and environmental changes during the past millennium in central western Guizhou, China as recorded by Stalagmite ZJD-21. J. Asian Earth Sci. 40, 1111–1120.
Lambert, W.J., Aharon, P., 2011. Controls on dissolved inorganic carbon and $\delta^{13}C$ in cave waters from DeSoto Caverns: implications for speleothem $\delta^{13}C$ assessments. Geochim. Cosmochim. Acta 75, 753–768.
Li, H.C., Lee, Z.H., Wan, N.J., Shen, C.C., Li, T.Y., Yuan, D.X., Chen, Y.H., 2011. The δO and δC records in an aragonite stalagmite from Furong Cave, Chongqing, China: a-2000-year record of monsoonal climate. J. Asian Earth Sci. 40, 1121–1130.
Li, J.-Y., Li, T.-Y., 2018. Seasonal and annual changes in soil/cave air $pCO_2$ and the $\delta^{13}C_{DIC}$ of cave drip water in response to changes in temperature and rainfall. Appl. Geochem. 93, 94–101.
Li, T.-Y., Huang, C.-X., Tian, L., Suarez, M., Gao, Y., 2018. Variation of $\delta^{13}C$ in plant-soil-cave systems in karst regions with different degrees of rocky desertification in southwest China. J. Cave Karst Stud. 80, 212–228.
Li, T., Li, H., Xiang, X., Kuo, T.-S., Li, J., Zhou, F., Chen, H., Peng, L., 2012. Transportation characteristics of $\delta^{13}C$ in the plants-soil-bedrock-cave system in Chongqing karst area. Sci. China Earth Sci. 55, 685–694.
Liu, C., Wei, Y., Liu, Y., Guo, K., 2009. Biomass of canopy and shrub layers of karst forest in Puding, Guizhou, China. Chin. J. Plant Ecol. 698–705.
Liu, D., Chen, Y., Cai, W., Dong, W., Xiao, J., Chen, J., Zhang, H., Xia, J., Yuan, W., 2014. The contribution of China's Grain to Green Program to carbon sequestration. Landscape Ecol. 29, 1675–1688.
Liu, D., Wang, Y., Cheng, H., Edwards, R.L., Kong, X., Li, T.-Y., 2017. Strong coupling of centennial-scale changes of Asian monsoon and soil processes derived from stalagmite $\delta^{18}O$ and $\delta^{13}C$ records, southern China. Quat. Res. 85, 333–346.
Liu, X., Liu, J., Chen, S., Chen, J., Zhang, X., Yan, J., Chen, F., 2020. New insights on Chinese cave δ18O records and their paleoclimatic significance. Earth-Sci. Rev. 207.
Luo, W., Wang, S., 2008. Transmission of oxygen isotope signals of precipitation-soil water-drip water and its implications in Liangfeng Cave of Guizhou, China. Sci. Bull.

53, 3364–3370.
Luo, W., Wang, S., Xie, X., 2013. A comparative study on the stable isotopes from precipitation to speleothem in four caves of Guizhou, China. Geochemistry 73, 205–215.
Luo, W., Wang, S., Zeng, G., Zhu, X., Wei, L., 2014. Daily response of drip water isotopes to precipitation in Liangfeng Cave, Guizhou Province, SW China. Quat. Int. 349, 153–158.
Lyu, Y., Luo, W., Wang, Y., Zeng, G., Wang, Y., Cheng, A., Zhang, L., Chen, J., Cai, X., Zhang, R., Wang, S., 2020. Impacts of cave ventilation on drip water $\delta^{13}C_{DIC}$ and its paleoclimate implication. Quat. Int. 547, 7–21.
Mattey, D., Lowry, D., Duffet, J., Fisher, R., Hodge, E., Frisia, S., 2008. A 53 year seasonally resolved oxygen and carbon isotope record from a modern Gibraltar speleothem: reconstructed drip water and relationship to local precipitation. Earth Planet. Sci. Lett. 269, 80–95.
Mattey, D.P., Atkinson, T.C., Barker, J.A., Fisher, R., Latin, J.P., Durrell, R., Ainsworth, M., 2016. Carbon dioxide, ground air and carbon cycling in Gibraltar karst. Geochim. Cosmochim. Acta 184, 88–113.
Mattey, D.P., Fairchild, I.J., Atkinson, T.C., Latin, J.-P., Ainsworth, M., Durell, R., 2010. Seasonal microclimate control of calcite fabrics, stable isotopes and trace elements in modern speleothem from St Michaels Cave, Gibraltar. Geol. Soc. London Spec. Publ. 336, 323–344.
McDermott, F., 2004. Palaeo-climate reconstruction from stable isotope variations in speleothems: a review. Quat. Sci. Rev. 23, 901–918.
McDonald, J., Drysdale, R., 2007. Hydrology of cave drip waters at varying bedrock depths from a karst system in southeastern Australia. Hydrol. Process 21, 1737–1748.
Meyer, K.W., Feng, W., Breecker, D.O., Banner, J.L., Guilfoyle, A., 2014. Interpretation of speleothem calcite $\delta^{13}C$ variations: evidence from monitoring soil $CO_2$, drip water, and modern speleothem calcite in central Texas. Geochim. Cosmochim. Acta 142, 281–298.
Moerman, J.W., Cobb, K.M., Partin, J.W., Meckler, A.N., Carolin, S.A., Adkins, J.F., Lejau, S., Malang, J., Clark, B., Tuen, A.A., 2014. Transformation of ENSO-related rainwater to dripwater $\delta^{18}O$ variability by vadose water mixing. Geophys. Res. Lett. 41, 7907–7915.
Pérez-Mejías, C., Moreno, A., Sancho, C., Bartolomé, M., Stoll, H., Osácar, M.C., Cacho, I., Delgado-Huertas, A., 2018. Transference of isotopic signal from rainfall to dripwaters and farmed calcite in Mediterranean semi-arid karst. Geochim. Cosmochim. Acta 243, 66–98.
Qi, X., Wang, K., Zhang, C., 2013. Effectiveness of ecological restoration projects in a karst region of southwest China assessed using vegetation succession mapping. Ecol. Eng. 54, 245–253.
Reddy, M.M., Schuster, P., Kendall, C., Reddy, M.B., 2006. Characterization of surface and ground water $\delta^{18}O$ seasonal variation and its use for estimating groundwater residence times. Hydrol. Process. 20, 1753–1772.
Riechelmann, D.F.C., Schröder-Ritzrau, A., Scholz, D., Fohlmeister, J., Spötl, C., Richter, D.K., Mangini, A., 2011. Monitoring Bunker Cave (NW Germany): a prerequisite to interpret geochemical proxy data of speleothems from this site. J. Hydrol. 409, 682–695.
Riechelmann, S., Schröder-Ritzrau, A., Spötl, C., Riechelmann, D.F.C., Richter, D.K., Mangini, A., Frank, N., Breitenbach, S.F.M., Immenhauser, A., 2017. Sensitivity of Bunker Cave to climatic forcings highlighted through multi-annual monitoring of rain-, soil-, and dripwaters. Chem. Geol. 449, 194–205.
Rutlidge, H., Baker, A., Marjo, C.E., Andersen, M.S., Graham, P.W., Cuthbert, M.O., Rau, G.C., Roshan, H., Markowska, M., Mariethoz, G., Jex, C.N., 2014. Dripwater organic matter and trace element geochemistry in a semi-arid karst environment: implications for speleothem paleoclimatology. Geochim. Cosmochim. Acta 135, 217–230.
Spötl, C., Fairchild, I.J., Tooth, A.F., 2005. Cave air control on dripwater geochemistry, Obir Caves (Austria): implications for speleothem deposition in dynamically ventilated caves. Geochim. Cosmochim. Acta 69, 2451–2468.
Sun, Z., Yang, Y., Zhao, J., Tian, N., Feng, X., 2018. Potential ENSO effects on the oxygen isotope composition of modern speleothems: observations from Jiguan Cave, central China. J. Hydrol. 566, 164–174.
Surić, M., Lončarić, R., Bočić, N., Lončar, N., Buzjak, N., 2018. Monitoring of selected caves as a prerequisite for the speleothem-based reconstruction of the Quaternary environment in Croatia. Quat. Int. 494, 263–274.
Tong, X., Wang, K., Yue, Y., Brandt, M., Liu, B., Zhang, C., Liao, C., Fensholt, R., 2017. Quantifying the effectiveness of ecological restoration projects on long-term vegetation dynamics in the karst regions of Southwest China. Int. J. Appl. Earth Obs. Geoinf. 54, 105–113.
Tooth, A.F., Fairchild, I.J., 2003. Soil and karst aquifer hydrological controls on the geochemical evolution of speleothem-forming drip waters, Crag Cave, southwest Ireland. J. Hydrol. 273, 51–68.
Treble, P., Shelley, J.M.G., Chappell, J., 2003. Comparison of high resolution sub-annual records of trace elements in a modern (1911–1992) speleothem with instrumental climate data from southwest Australia. Earth Planet. Sci. Lett. 216, 141–153.
Treble, P.C., Bradley, C., Wood, A., Baker, A., Jex, C.N., Fairchild, I.J., Gagan, M.K., Cowley, J., Azcurra, C., 2013. An isotopic and modelling study of flow paths and storage in Quaternary calcarenite, SW Australia: implications for speleothem paleoclimate records. Quat. Sci. Rev. 64, 90–103.
Treble, P.C., Fairchild, I.J., Baker, A., Meredith, K.T., Andersen, M.S., Salmon, S.U., Bradley, C., Wynn, P.M., Hankin, S.I., Wood, A., McGuire, E., 2016. Roles of forest bioproductivity, transpiration and fire in a nine-year record of cave dripwater chemistry from southwest Australia. Geochim. Cosmochim. Acta 184, 132–150.
Velbel, M.A., Price, J.R., 2007. Solute geochemical mass-balances and mineral weathering rates in small watersheds: methodology, recent advances, and future directions. Appl. Geochem. 22, 1682–1700.
Wallacke, A., Mueller, R.T., Wood, R.A., Soufi, S.M., 1979. Plant uptake of bicarbonate as measured with the $^{11}C$ isotope. Plant Soil 51, 431–435.
Wang, K., Wang, P., Liu, J., Sparrow, M., Haginoya, S., Zhou, X., 2005. Variation of surface albedo and soil thermal parameters with soil moisture content at a semi-desert site on the western Tibetan Plateau. Bound.-Layer Meteorol. 116, 117–129.
Wang, X., Guan, H., Huo, Z., Guo, P., Du, J., Wang, W., 2020a. Maize transpiration and water productivity of two irrigated fields with varying groundwater depths in an arid area. Agric. Forest Meteorol. 281.
Wang, Y., Luo, W., Zeng, G., Peng, H., Cheng, A., Zhang, L., Cai, X., Chen, J., Lyu, Y., Yang, H., Wang, S., 2020b. Characteristics of carbon, water, and energy fluxes on abandoned farmland revealed by critical zone observation in the karst region of southwest China. Agric. Ecosyst. Environ. 292, 106821.
Wassenburg, J.A., Riechelmann, S., Schröder-Ritzrau, A., Riechelmann, D.F.C., Richter, D.K., Immenhauser, A., Terente, M., Constantin, S., Hachenberg, A., Hansen, M., Scholz, D., 2020. Calcite Mg and Sr partition coefficients in cave environments: Implications for interpreting prior calcite precipitation in speleothems. Geochim. Cosmochim. Acta 269, 581–596.
Wong, C.I., Banner, J.L., Musgrove, M., 2011. Seasonal dripwater Mg/Ca and Sr/Ca variations driven by cave ventilation: implications for and modeling of speleothem paleoclimate records. Geochim. Cosmochim. Acta 75, 3514–3529.
Woo, K.S., Ji, H., Jo, K.N., Yi, S., Cheng, H., Edwards, R.L., Hong, G.H., 2015. Reconstruction of the Northeast Asian monsoon climate history for the past 400 years based on textural, carbon and oxygen isotope record of a stalagmite from Yongcheon lava tube cave, Jeju Island, Korea. Quat. Int. 384, 37–51.
Wu, Y., Li, T.-Y., Yu, T.-L., Shen, C.-C., Chen, C.-J., Zhang, J., Li, J.-Y., Wang, T., Huang, R., Xiao, S.-Y., 2020. Variation of the Asian summer monsoon since the last glacial-interglacial recorded in a stalagmite from southwest China. Quat. Sci. Rev. 234, 106261.
Wynn, P.M., Borsato, A., Baker, A., Frisia, S., Miorandi, R., Fairchild, I.J., 2012. Biogeochemical cycling of sulphur in karst and transfer into speleothem archives at Grotta di Ernesto, Italy. Biogeochemistry 114, 255–267.
Yang, T., Wang, S., Luo, W., Xie, X., Xiao, D., Li, T., Zhou, Y., 2012. A new tracer ($SO_4$) in modern environmental monitoring study. Earth Environ. 40, 1–8.
Yonge, C.J., Ford, D.C., Gray, J., Schwarcz, H.P., 1985. Stable isotope studies of cave seepage water. Chem. Geol. Isotope Geosci. 58, 97–105.
Zhang, J., Li, T.-Y., 2019. Seasonal and interannual variations of hydrochemical characteristics and stable isotopic compositions of drip waters in Furong Cave, southwest China based on 12 years' monitoring. J. Hydrol. 572, 40–50.
Zhou, Y., Wang, S., 2005. Hydrogeochemical process of cave drips study on Xiniu Cave, Zhenning, Guizhou. Earth Environ. 33, 23–30.